Available online at www.sciencedirect.com
ScienceDirect
Engineering Fracture Mechanics 73 (2006) 2662–2684
Engineering Fracture Mechanics
www.elsevier.com/locate/engfracmech

A weight function methodology for the assessment of embedded and surface irregular plane cracks

Hugo López Montenegro *, Adrián Cisilino, José Luis Otegui

Institute of Materials Science and Technology (INTEMA), University of Mar del Plata, Welding and Fracture Division, J. B. Justo 4302, 7600 Mar del Plata, Buenos Aires, Argentina

Received 20 September 2005; received in revised form 2 April 2006; accepted 12 April 2006
Available online 14 June 2006

Abstract

A low cost numerical tool for the calculation of mode I stress intensity factors K in embedded and surface irregular cracks is presented in this paper. The proposed tool is an extension of the O-integral algorithm due to Oore and Burns for the assessment of embedded plane cracks using the weight function methodology. The performance of the O-integral is assessed first by comparing its K results to exact solutions for embedded elliptical and rectangular cracks. From the analysis of this data it is found that the error in the K results systematically depends on the crack aspect ratio and the local crack front curvature. Based on this evidence a corrective function is derived in order to remediate the limitations of the O-integral. Solutions due to Newman and Raju are used to account for the effects of free surfaces and finite thickness. The accuracy of the proposed procedure is assessed by solving a number of examples and by comparing the obtained results to those available in the literature.

Keywords: Fracture mechanics; Stress intensity factor; Three-dimensional cracks; Numerical algorithms; Surface cracks

1. Introduction

Design standards based on theory and rules of good art allow to minimize the risk of failure of structures of all types. Among those, best known are ASME PVPC Code [1], used by manufacturers and operators of pressure vessels and pipes, and others applicable to specific industries. These standards mostly come from USA (API, SEAL, STUMP, etc.), and from European countries (DIN, ISO, etc.). Another interesting aspect refers to the evaluation of equipment in operation that, due to fabrication errors or accumulated damage in service, show discontinuities or crack-like defects that are not allowed by the manufacturing codes. Nowadays there is an advanced theoretical understanding and an array of experimental and numerical tools to address this engineering problem; such as failure analyses, root cause assessments, testing of laboratory samples, numerical analysis for design and re-rating, etc. A set of documents and recommended practices standardize the analysis

* Corresponding author. Tel.: +54 223 4816600; fax: +54 223 4810046.
E-mail address: hmonte@fi.mdp.edu.ar (H.L. Montenegro).

0013-7944/$ - see front matter © 2006 Elsevier Ltd. All rights reserved.
doi:10.1016/j.engfracmech.2006.04.007

Nomenclature

a, c	crack dimensions: half depth and half width, respectively
r, r^*	crack aspect ratio
b	half width of a plate
t	plate thickness
K	stress intensity factor
K_{corr}	corrected stress intensity factor
K_I	mode I stress intensity factor
$K_{Q'}$	stress intensity factor at a point Q' on the crack front
σ	opening stress
σ_0	remote uniform stress
σ_Q	opening force intensity (pressure) at a point Q
A	crack surface area
s	crack front
ds	elemental length of the crack front s
$l_{QQ'}$	distance from the load point Q to the point Q' on the crack front
ρ_Q	distance from point Q to the center of the elemental length ds
$W_{QQ'}$	weight function
χ_n	non-dimensional normalized curvature of the crack front
ϕ	parametric angle for the crack geometry
$r(\theta)$, θ	polar coordinates
f_c	corrective function
P, R, G	defined functions of r
f_1, f_2	defined functions of χ_n
p, q, t	coefficients in f_2, depending on the parameter r
Y	configuration function
Y_b	configuration function for the crack in an infinite body
Y_b^C	Y_b solution obtained by using the Calyf program
λ_s	free surface correction factor
f_ϕ	Newman and Raju solution function for an ambedded elliptical crack
Q	parameter approximating the square of the elliptical integral of second type
F_S, H	Newman and Raju auxiliary functions
σ_m, σ_b	remote membrane and pure bending stresses, respectively
t_m, t_b	normalized values of σ_m and σ_b, respectively
f_S	auxiliary function for F_S
g_S, f_w	auxiliary functions for f_S
M^S	auxiliary parameters for f_S
q	parameter related to the deformation of a circumference of radius one

of structures in service, which purpose is to prevent accidents and at the same time to reduce repair costs. The British documents BSI PD 6493 [2], CEGB R6 [3]; and the American documents EPRI (Electric Power Research Institute) of 1981 and 1990 [4,5] were among the first bodies to address the problem, leading to present day procedures such as the British Standard BS 7910 [6], which replaces the PD 6493, the European standard procedure for structural integrity assessment SINTAP [7] and the American Petroleum Institute Recommended Practice API RP 579 [8].

Assessing the engineering integrity and life expectancy of a cracked component or structure, either under service conditions or during the design stage requires the determination of fracture parameters as the stress intensity factor K. In this sense, most of the above-mentioned codes and standard procedures use assessment rules with a certain degree of conservatism. For example, API RP 579 models embedded or surface cracks as

ellipses or semi-ellipses, respectively, based on their width and depth, as they could be defined by ultrasonic non-destructive testing. Similar approaches are applied to through cracks in the center or edge of a plate, where the irregular geometry of the crack front is idealized as a straight fronted crack. In the case of a corner crack, it is idealized as a quarter ellipse. With respect to multiple cracks, all documents establish approaches for crack interaction.

Another well-established criterion to estimate stress intensity factors for simple cracks of arbitrary geometry, is in terms of $\sqrt{\text{Area}}$. Following this approach, Murakami et al. [9,10] proposed simple formulas for the estimation of K maximum values in surface or embedded cracks, with a reported accuracy of 10%. In a recent work, Noda [11] checks the validity of these formulas in rectangular and elliptical cracks of different aspect ratios, and extends them to the case of mixed mode loading in homogeneous and heterogeneous materials.

When a K solution is required for a crack of arbitrary shape in a complex structural configuration methods based on finite elements (FEM) or boundary elements (BEM) are widely applicable [12]. Although very effective, versatile, and capable of delivering solutions with a high level of accuracy, the drawback of these methods is their relatively high computing cost and time needed for the model preparation.

Since the introduction of the weight function concept to crack problems by Bueckner [13] and Rice [14], many numerical methods have emerged for the calculation of stress intensity factors. Weight function methodologies are simple and accurate, but they present the drawback that a particular weight function solution is necessary for each model geometry. This feature limits the applicability of the methodology, especially in the case of three-dimensional problems, for which available weight function solutions are limited to simple regular geometries [15]. In an effort to extend the applicability of the weight function methodology, Oore and Burns [16] proposed a general, geometrically defined weight function for calculating the opening mode stress intensity factor at any point on the front of an irregular planar crack embedded in an infinite solid subjected to an arbitrary stress field. This methodology known as the O-integral has proved general and versatile. However, depending on the local crack-front curvature, it could deliver K results with errors of up to 20% for simple geometries such as elliptical cracks with low aspect ratios.

A corrective procedure to extend the applicability of the O-integral methodology is introduced in this paper. In a first step, the performance of the O-integral is assessed and a correction function proposed in order to remediate accuracy problems referenced in the previous paragraph. In a second step, a corrective procedure is presented to allow the O-integral for the analysis of surface cracks and to account for the effect of finite thickness. The accuracy of the procedure is assessed by studying a number of examples and comparing their results to solutions obtained using BEM models and available in the literature.

2. The O-integral

According to the weight function (WF) concept [13], for an opening force intensity (pressure) σ_Q acting on the crack surface area A, the stress intensity factor $K_{Q'}$ at a point Q' on the crack front is an integral calculated on the crack surface area as

$$K_{Q'} = \int_A \sigma_Q \cdot W_{QQ'} \cdot \mathrm{d}A \tag{1}$$

where $W_{QQ'}$ is the weight function, which depends on the problem geometry only. It is worth mentioning that most of the available weight function solutions are limited to two-dimensional cracks and regular crack geometries in three-dimensions [15], what certainly limits the scope of problems which can be solved using this technique.

In an effort to extend the applicability of the weight function methodology, Oore and Burns [16] examined the structure of the weight functions for three-dimensional cracks for which there are known solutions, and surmised that in general these weight functions could be rewritten as, or approximated by

$$W_{QQ'} = \frac{\sqrt{2}}{\pi \cdot l_{QQ'}^2} \cdot \frac{1}{\left[\int_S \frac{\mathrm{d}s}{\rho_Q^2}\right]^{1/2}} \tag{2}$$

where $l_{QQ'}$ is the distance from the load point Q to the point Q' on the crack front, and ρ_Q is the distance from Q to the center of the elemental length ds of the crack front s (see Fig. 1(a)). Thus, the O-integral is a geometrically defined weight function for calculating opening mode stress intensity factors at any point on the front of an irregular planar crack, embedded in an infinite solid and subjected to an arbitrary stress field [17].

It has been shown that this integral satisfactorily predicts K_I for a variety of normally loaded, embedded cracks. Among others, particular solutions have been derived for a circular crack with a pair of opening, symmetrical, point loads, an elliptical crack under uniform or linear varying stress field, an annular circular crack in a uniform stress field, and a parabolic crack in a uniform stress field [16]. For some of the aforementioned test cases, it was possible to obtain closed-form solutions for Eq. (1).

In the case of cracks of arbitrary shape and loading, the O-integral needs to be evaluated numerically. In this sense, Desjardins [17] proposed a numerical algorithm that employs interior and border elements for the discretization of the crack surface area (see Fig. 1(b)). For the interior elements the evaluation of the integral

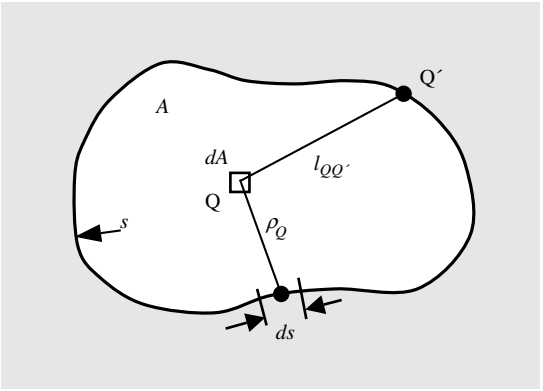

(a)

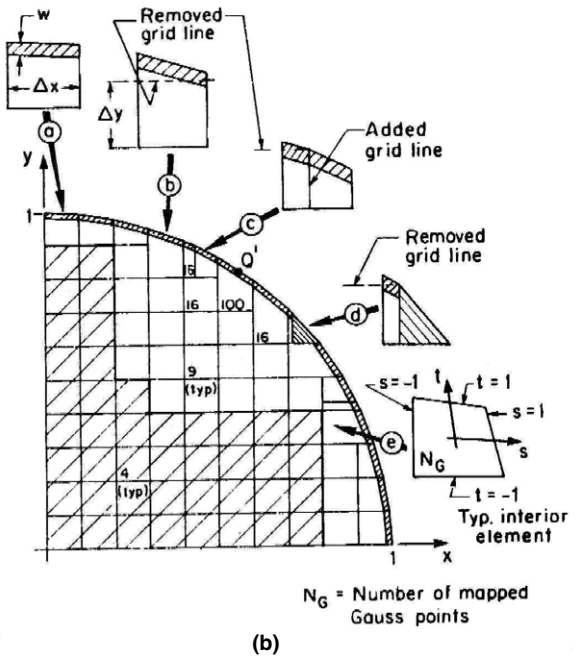

(b)

Fig. 1. (a) Definition of geometric variables used in the O-integral, (b) discretization strategy. Note the utilization of boundary and interior elements used by Desjardins (from Ref. [17]).

in Eq. (1) is carried out using the standard Gauss integration formula, while for the border elements the solution is obtained by means of a semi-analytical procedure.

Although general and versatile, it is found that depending on the local crack-front curvature, K results are systematically under or overestimated by the O-integral. In the following section the performance of the O-integral is assessed and a corrective function proposed in order to remediate the above-mentioned limitation. In the same way a corrective procedure is introduced in order to extend the applicability of the methodology to surface cracks and finite-thickness specimens.

3. Assessment and improvement of the O-integral

3.1. Embedded cracks

Elliptical and rectangular cracks were selected to assess the precision of the O-integral. Exact solutions for the elliptical crack in an infinite domain are documented in the literature; the Irwin solution for uniform remote tension [18] and the Shah and Kobayashi solution for pure bending [19].

In the work by Desjardin [17], circular and elliptical cracks under tension and bending stresses were solved using the O-integral, and the results compared with the exact solutions. Maximum errors were found to be almost independent from the loading case, but dependent on crack geometry. Maximum error was found 0.65% for the circular crack, while for elliptical cracks the error monotonically increased with the diminution of the crack aspect ratio (the ratio between the length of the minor and the major axes of the ellipse). Maximum error was found in the later case equal to 18.38% for an elliptical crack of aspect ratio 0.2. This behavior allows us to conclude that in the circumferential crack the error can be entirely attributed to the numerical algorithm, as for this geometry the O-integral solution matches exactly the analytical weight function. In contrast, for the elliptical crack the largest error corresponds to the portion of the crack front with largest curvature. Convergence analyses done using different discretizations showed that this error is due to the O-integral formulation itself, not a consequence of the numerical evaluation. The fact that the error changes monotonically with the ellipse aspect ratio and the local crack front curvature suggests the possibility of obtaining a corrective function for K which depends on these two parameters only.

The aspect ratio of the ellipse with half axes c and a, is defined as $r = a/c$. At the same time, the non-dimensional normalized curvature χ_n (from now on, simply referred as 'curvature') at a generic front point Q' associated with the parameter ϕ (see Fig. 2) is given by Eq. (3):

$$\chi_n(\phi) = \frac{(a/c)^2}{\left[\sin^2(\phi) + (a/c)^2 \cdot \cos^2(\phi)\right]^{\frac{3}{2}}} \tag{3}$$

For ellipses with aspect ratio $r \leqslant 1$, the curvature diminishes monotonically with the parameter ϕ, and it presents extreme values given by

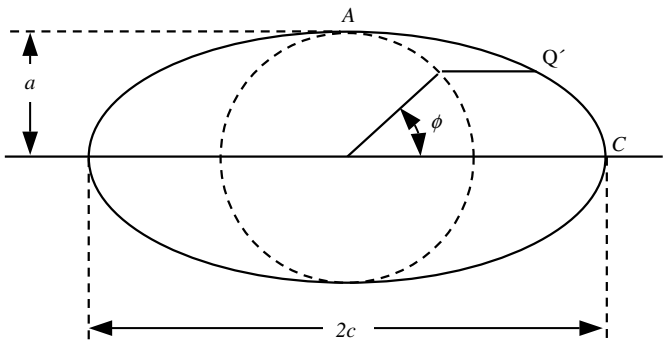

Fig. 2. Elliptical crack and its characteristic geometrical parameters.

$$\chi_n(0) = 1/r; \quad \chi_n(\pi/2) = r^2 \tag{4}$$

where $\phi = 0$ corresponds to the major curvature of the ellipse (point C), and $\phi = \pi/2$ to the minor curvature (point A) in Fig. 2. The corrective function f_c is defined as

$$f_c(r, \chi_n) = \frac{K(\text{reference solution})}{K(\text{Oore})} \tag{5}$$

Then, the corrected stress intensity factor value K_{corr} results from the product of the K(Oore) value and the corrective function f_c

$$K_{corr} = K(\text{Oore}) \cdot f_c \tag{6}$$

When the corrective function is calculated as a function of the crack front curvature for elliptical cracks with aspect ratios $0.2 \leqslant r \leqslant 1$, the set of curves shown in Fig. 3 is obtained. Exact solutions due to Irwin [18] were used as reference in this case. As seen in the figure, all the curves are approximately parallel for curvatures $\chi_n \geqslant 1$. At the same time, as the aspect ratio approximates to one, the curves converge to the limiting point L, which corresponds to a circumferential crack with constant curvature $\chi_n = 1$ and corrective function $f_c = 1$.

The K solutions of rectangular cracks given by Isida et al. [20] were employed as reference solutions to study the behavior of the corrective function for geometries with null curvature and different aspect ratios. Isida solutions, obtained by means of the body force method, allow computing K_I at point A on the crack front (see subfigure in Fig. 4) with a maximum error less than 1%. The corrective function for the rectangular cracks is plotted in Fig. 4. It can be appreciated that f_c approximates to one as r tends to zero. This behavior is coherent with the Oore and Isida solutions. It is worth to note here that the geometrical WF proposed by Oore exactly matches the closed form solution of the WF for a 3-D tunnel crack in an infinite solid or the centered crack in a 2-D infinite plate [16].

Based upon the analysis of the above results, an algorithm for the computation of the corrective function f_c is proposed next. The scheme in Fig. 5 illustrates the typical behavior of the curves plotted in Fig. 3, which present the maximum value of f_c in the position with minimum curvature, $\chi_n = r^2$. Two points are defined next: point R, which is given by the intersection of the curve and the vertical line $\chi_n = 1$; and point P, which corresponds to the intersection of the curve with the horizontal line $f_c = 1$. The abscissa of P and the ordinate of R were computed for all the curves in Fig. 3 ($0.2 \leqslant r < 1$) using data interpolation. Obtained results are presented in Fig. 6 as a function of the crack aspect ratio r. Fig. 6(a) corresponds to the results for the ordinate

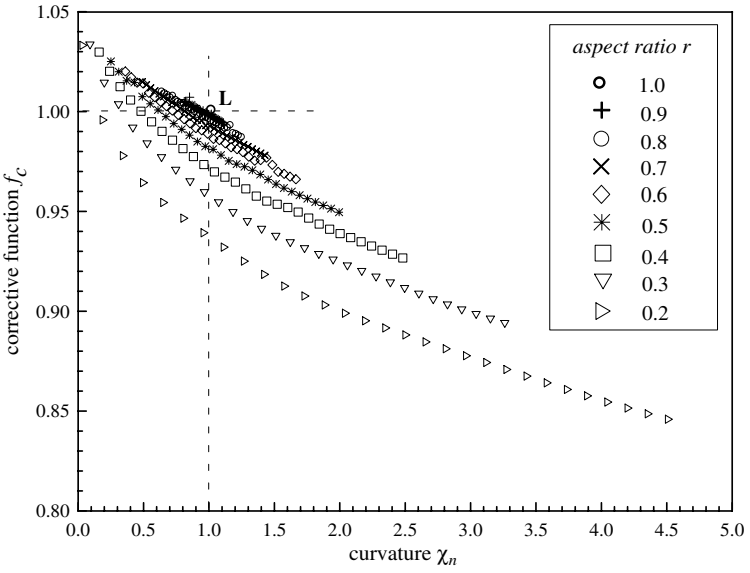

Fig. 3. Corrective function for elliptical crack as a function of the curvature.

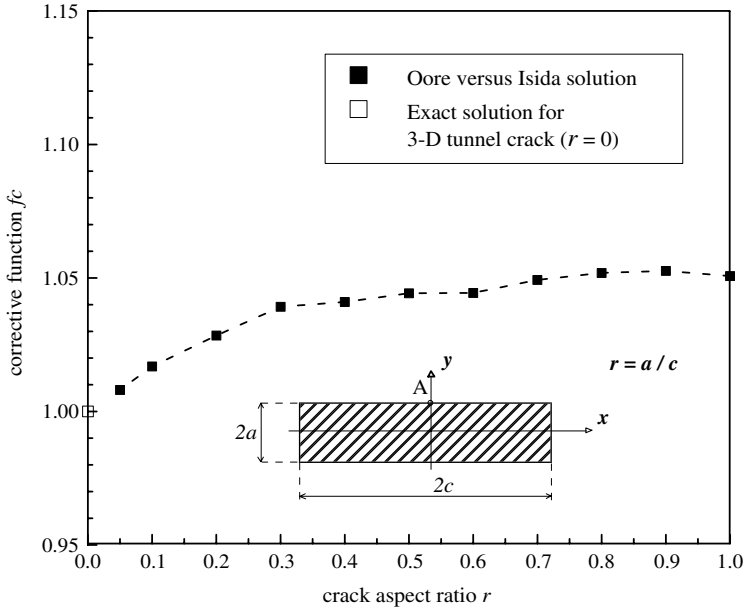

Fig. 4. Corrective function at point A for a family of rectangular cracks embedded in an infinite volume.

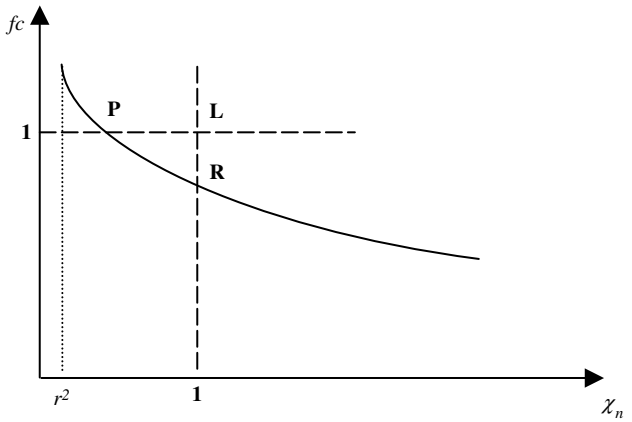

Fig. 5. Scheme of a typical curve reported in Fig. 3 for a given aspect ratio $0.2 \leqslant r < 1$.

of point R, function $R(r)$, while Fig. 6(b) illustrates the results for the abscissa of point P, function $P(r)$. The best fitting functions $R(r)$ and $P(r)$ are given in Eqs. (7) and (8), respectively

$$R(r) = 0.8915 + 0.2953 \cdot r - 0.2773 \cdot r^2 + 0.0905 \cdot r^3 \tag{7}$$

$$P(r) = 0.839 \cdot r; \quad 0 \leqslant r < 0.2 \tag{8a}$$

$$P(r) = -0.278554 + 2.58316 \cdot r - 1.78777 \cdot r^2 + 0.483164 \cdot r^3; \quad 0.2 \leqslant r \leqslant 1 \tag{8b}$$

Note that since $f_c = 1$ for $r = 0$ for both the rectangular and elliptical cracks, the function $P(r)$ was linearly approximated in the range $0 \leqslant r < 0.2$ (see Fig. 6(b)). On the other hand, the function $R(r)$ was extrapolated for $r < 0.2$ (see Fig. 6(a)). It is also worth noting that for $r = 1$, both $P(r)$ and $R(r)$ tend to one, i.e., the limiting point L (see Fig. 5).

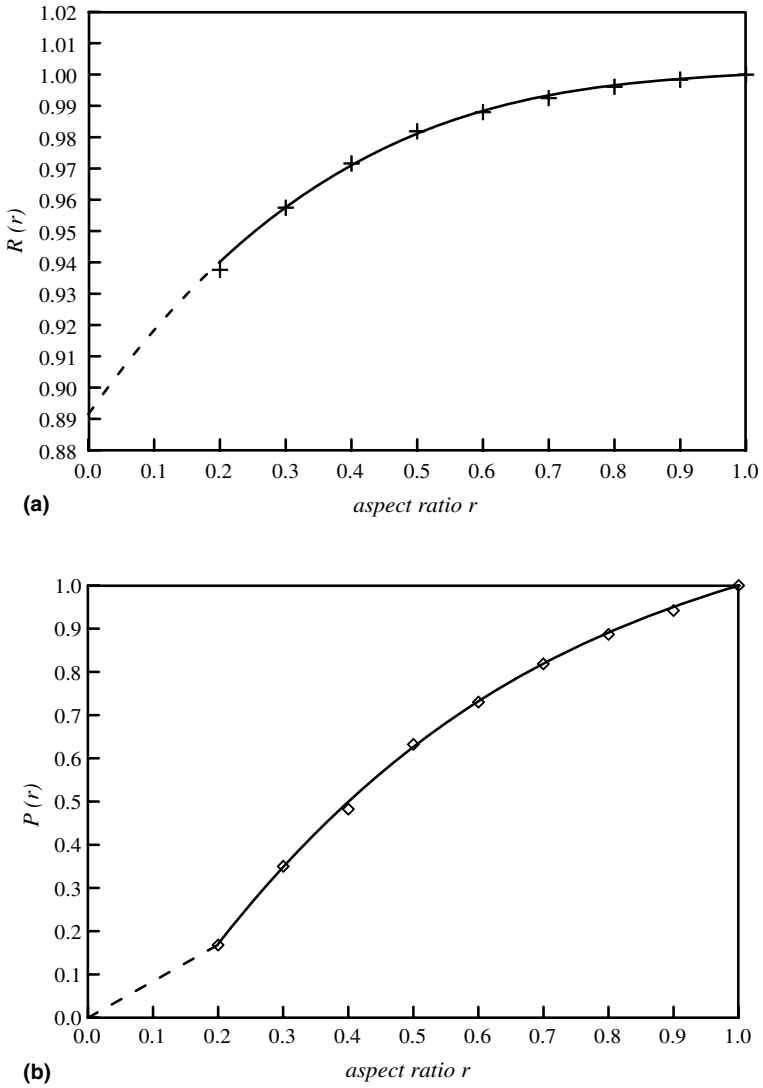

Fig. 6. Intersection functions for ellipses: (a) ordinate $R(r)$, (b) abscissa $P(r)$.

As it was mentioned before, curves in Fig. 3 result approximately parallel for curvatures $\chi_n > 1$. Thus, data with $\chi_n > 1$ for all the curves in Fig. 3 was shifted to contain point L by using Eq. (7). Then, a single exponential function $f_1(\chi_n)$ was obtained by fitting all the data (see Eq. (9) and continuous line in Fig. 7)

$$f_1(\chi_n) = 0.85076 + 0.23245 \cdot \exp\left[\frac{-(\chi_n + 0.68767)}{3.80872}\right] \tag{9}$$

Similarly, data with abscissa $\chi_n < 1$ and only for the curves in the range $0.7 \leqslant r \leqslant 0.9$ was also shifted to contain point L. As it can be seen from Fig. 7, this data is adequately represented by the extrapolation of the exponential fit given in Eq. (9) (see dashed line in Fig. 7). On the other hand, data in the curves of Fig. 3 for $r < 0.7$ does not follow the same pattern, and thus, an alternative fitting scheme for these curves is necessary for $\chi_n < 1$. Best results in this case were obtained using a parabolic interpolation function $f_2(\chi_n)$ with positive concavity as follows:

$$f_2(\chi_n) = p \cdot \chi_n^2 + q \cdot \chi_n + t \tag{10}$$

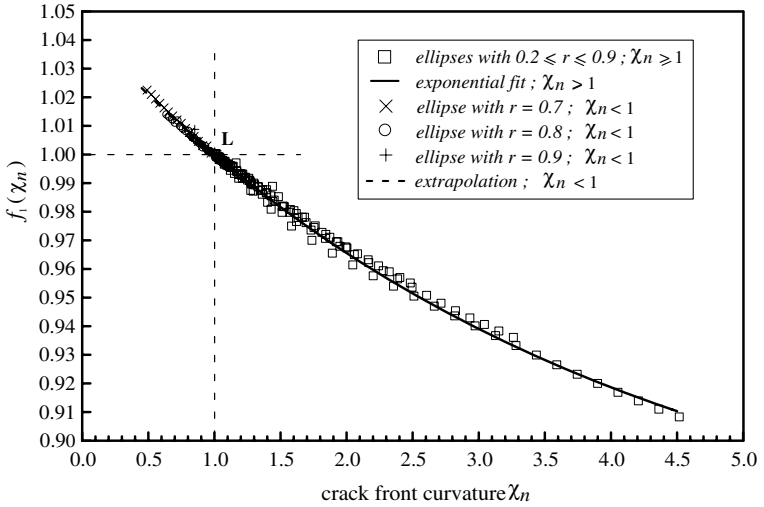

Fig. 7. Data from Fig. 3 transferred on the basis of Eq. (7) and the exponential function $f_1(\chi_n)$.

with coefficients depending on the parameter r by

$$p = \frac{1 + G(r) - R(r) - G(r)\cdot P(r)}{(P(r)-1)^2}$$

$$q = \frac{G(r)\cdot (P^2(r)-1) + 2R(r) - 2}{(P(r)-1)^2}$$

$$t = R(r) - p - q$$

where

$$G(r) = \frac{0.85076 - R(r)}{3.80872}$$

This selection of $f_2(\chi_n)$ ensures that the C^1 continuity condition is satisfied at $\chi_n = 1$ (i.e., both interpolation functions, $f_1(\chi_n)$ and $f_2(\chi_n)$, have the same slope at $\chi_n = 1$). In this way, the corrective function $fc(r, \chi_n)$ results in a piece-wise representation. It is worth to note that the C^1 condition and the requirement of positive concavity for $f_2(\chi_n)$ allow obtaining the exact value for $r^* = 0.6895$, the limiting point between the two fitting schemes. In this way, for cracks with aspect ratios $r \geqslant r^*$ the corrective function $fc(r, \chi_n)$ is computed by means of Eqs. (7) and (9). On the other hand, if $r < r^*$ the corrective function is computed using Eqs. (7) and (9) only when $\chi_n \geqslant 1$, while for $\chi_n < 1$ Eq. (10) is employed. Fig. 8 illustrates the later case.

Finally, the algorithm for the computation of the corrective function is as follows:

(a) Compute the crack aspect ratio, r.
(b) Compute the local curvature χ_n at the point of interest on the crack front. If $\chi_n < 0$, set $\chi_n = 0$.
(c) If $r \geqslant r^* = 0.6895$, compute the corrective function using Eqs. (7) and (9) by doing

$$f_c = f_1 - [1 - R(r)]$$

(d) If $r < r^*$, compute the corrective function using the procedure given in (c) for $\chi_n \geqslant 1$, or the function f_2 given in Eq. (10) for $\chi_n < 1$.

The O-integral numerical solver and the aforementioned algorithm were implemented in a program named Calsyf. Preliminary tests with the program have shown that the algorithm provides K results for elliptical and rectangular cracks under tension with errors less than 1.6% and 1.06%, respectively. This level of accuracy results very competitive when compared to other simple formulas for the estimation of maximum K values

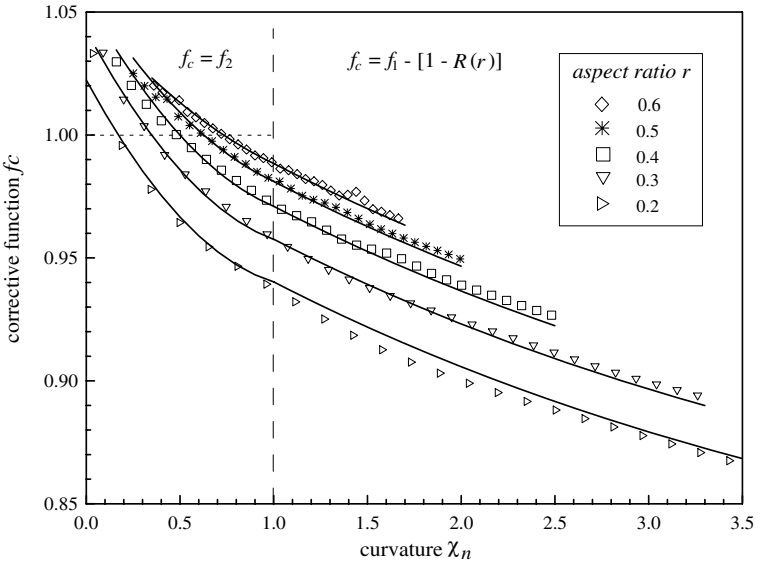

Fig. 8. Data from Fig. 3 for $r \leqslant 0.6$ and correcting function f_c defined from the fitting functions $f_1(\chi_n)$ and $f_2(\chi_n)$.

[9–11], with reported errors of a few percent. Finally, it is worth to mention that the proposed algorithm is not limited to regular crack geometries. As it will be shown later, the corrective function can be easily and successfully extended to solve irregular cracks.

3.2. Surface cracks

3.2.1. Introduction

The O-Integral was developed to solve embedded plane cracks in an infinite domain. However, practical fracture mechanics problems deal with surface cracks, mostly located in finite thickness plates or shells. In what follows an algorithm is proposed in order to extend the applicability of the O-integral methodology for the assessment of surface cracks located in semi-infinite bodies and in finite thickness geometries.

The generic expression of K in a point of the crack front is

$$K = Y\sigma\sqrt{\pi a} \tag{11}$$

where the non-dimensional factor "Y" is a normalized K, or configuration function, which depends on geometrical parameters and on the loading configuration. When treating surface cracks in a semi-infinite body, the Y factor can be split in two terms as follows:

$$Y \rightarrow \lambda_s \cdot Y_b$$

where factor λ_s accounts for the correction due to the free surface, and the function Y_b corresponds to the configuration function for the crack in an infinite body. Note that this approach allows using the program Calsyf to obtain the solution for Y_b, named Y_b^C, in arbitrary surface cracks under arbitrary loads, provided that λ_s for the given geometry is available. From Eqs. (6) and (11), the parameter Y_b^C is then expressed by

$$Y_b^C = \frac{K_{corr}}{\sigma\sqrt{\pi a}} \tag{12}$$

As it will be shown, this procedure can be extended to the treatment of finite width plates.

A usual procedure that simplifies the study of surface cracks subjected to arbitrary loads consists in computing the K solution for an equivalent embedded crack in an infinite body. This is done by considering the free surface as a plane of symmetry. The procedure is illustrated in Fig. 9 for an irregular surface crack. Note that for an irregular geometry like the one shown in Fig. 9, a generalized aspect ratio can be defined as the

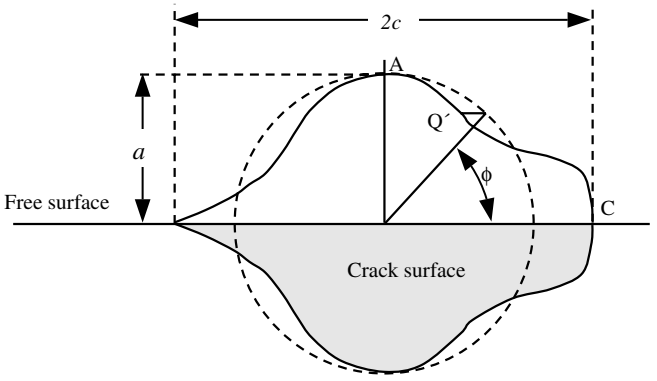

Fig. 9. Irregular surface crack and its equivalent symmetrical crack.

maximum axis ratio $\frac{2a}{2c}$. The O-integral applies the above procedure when dealing with arbitrary cracks and loads, as shown in the works of Oore and Burns [21] and of Grueter et al. [22], as a means to compute the Y_b factor.

3.2.2. Correction due to free surface and finite size geometry

In the resolution of elliptical or semi-elliptical surface cracks in a finite plate, the solution by Newman and Raju [23,24] is broadly used. This solution was obtained from finite element results, with reported accuracy of ±5%. Considering a function f_ϕ defined as

$$f_\phi = \left(\sin^2(\phi) + (a/c)^2\cos^2(\phi)\right)^{1/4} \tag{13}$$

the Newman and Raju solution for an elliptical crack in an infinite body under unitary uniform stress can be expressed as (see Appendix A for further details):

$$Y_b = f_\phi/\sqrt{Q} \tag{14}$$

where

$$Q = 1 + 1.464(a/c)^{1.65} \tag{15}$$

and the root $\sqrt{Q}$ approximates the elliptical integral of second type.

When a semi-elliptical crack in a semi-infinite volume under uniform stress is considered, the configuration function Y is given by

$$Y = \lambda_s \cdot Y_b \tag{16}$$

with the free surface correction factor λ_s (see Appendix B):

$$\lambda_s(\phi, a/c) = [1.13 - 0.09(a/c)] \cdot [1 + 0.1(1 - \sin(\phi))^2] \tag{17}$$

Therefore, the procedure proposed in this work for dealing with surface cracks in thick plates that can be assimilated to a semi-infinite domain consists in solving the equivalent embedded crack (see Section 3.2.1) to compute the factor Y_b^C (Eq. (12)) and using the correction factor λ_s (Eq. (17)) to account for the effect of the free surface. Then, the configuration function Y at a point in the crack front is expressed by

$$Y = \lambda_s(\phi, a/c) \cdot Y_b^C \tag{18}$$

Eq. (18) allows finding K for regular and irregular geometries; by defining the parameter ϕ associated to a point Q' of the crack front, as it is shown in Fig. 9. Point C in the surface corresponds to $\phi = 0°$, and for the deepest point A is $\phi = 90°$. Since the surface correction factor λ_s is a decreasing function of ϕ, the correction is larger for point C than for point A, as expected. Note that in the case of an elliptical crack, the definition given by the angular parameter coincides with the one given in Fig. 2.

For cases that involve finite geometries, Newman and Raju introduced auxiliary functions F_S and H which contemplates the proximity of borders. For a semi-elliptical crack of aspect ratio a/c located amid a finite plate of width $2b$ and thickness t (see Fig. 18(a) and (b) in Appendix B), the K solution for a linear normal stress field is expressed by

$$K = (\sigma_m + H \cdot \sigma_b)\sqrt{\frac{\pi a}{Q}} F_S(a/c, a/t, c/b, \phi) \tag{19}$$

where σ_m and σ_b are the remote membrane and pure bending stresses, respectively. Functions H and F_S both depend on the geometry parameters a/c, a/t, c/b, and on the angular parameter ϕ. The function F_S can be rewritten:

$$F_S = f_S(a/t, a/c, c/b, \phi) \cdot f_\phi(\phi, a/c) \tag{20}$$

where $f_\phi(\phi, a/c)$ has been defined in Eq. (13) and the function f_S is (see Appendix B for details)

$$f_S = \left[M_1^S + M_2^S\left(\frac{a}{t}\right)^2 + M_3^S\left(\frac{a}{t}\right)^4\right] \cdot g_S \cdot f_w \tag{21}$$

If σ_0 is the reference stress for a given problem, such as the stress in the most stressed point in the plate thickness, then

$$\sigma_m = t_m \cdot \sigma_0$$
$$\sigma_b = t_b \cdot \sigma_0$$

The configuration function Y can be expressed in terms of the non-dimensional magnitudes t_m and t_b as follows

$$Y = \frac{K}{\sigma_0\sqrt{\pi a}} = (t_m + H t_b) f_S \frac{f\phi}{\sqrt{Q}} \tag{22}$$

Then, from Eq. (14), it follows

$$Y = (t_m + H t_b) f_S Y_b \tag{23}$$

where Y_b is the configuration function of the equivalent crack located in an infinite body under unit uniform stress, and the pre-factors in the equation account for the corrections due to the free surface, loads and the plate geometry.

The application of the above procedure to the case of arbitrary cracks in finite plates is immediate. By substituting the factor Y_b by the factor Y_b^C given by Calsyf for the equivalent crack:

$$Y = (t_m + H t_b) f_S Y_b^C \tag{24}$$

In this way, the stress intensity factor K for surface crack of arbitrary shape under remote membrane and pure bending stresses can be solved by using the previously defined parameters and the Calsyf solution Y_b^C:

$$K = \sigma_0\sqrt{\pi a}(t_m + H t_b) f_S Y_b^C \tag{25}$$

4. Results and discussion

4.1. Embedded cracks of irregular front

In order to evaluate the performance of the proposed corrective algorithm, two examples consisting of irregular crack geometries embedded in an infinite body are studied next.

The first example consists in the crack geometry referred as "curvan", which is generated using the function:

$$r(\theta) = 1 + q \cdot \cos(4 \cdot \theta) \tag{26}$$

where the parameter "q" is related to the "deformation" of a circumference of radius one (note from Eq. (26) that $q = 0$ results in a circumference). Fig. 10 illustrates the crack geometry for $q = 0.1$. The parameter ϕ is the same defined in Fig. 2. The analytic definition of the crack geometry allows computing the crack front curva-

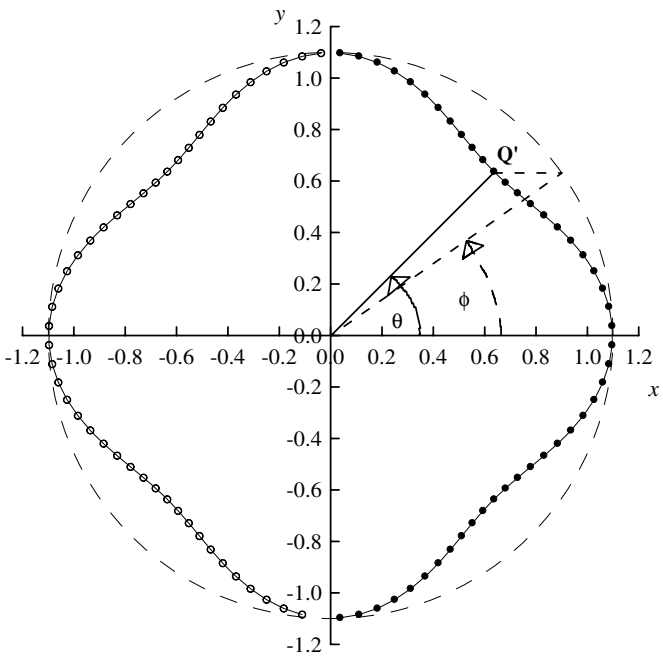

Fig. 10. Curvan crack geometry ($q = 0.1$).

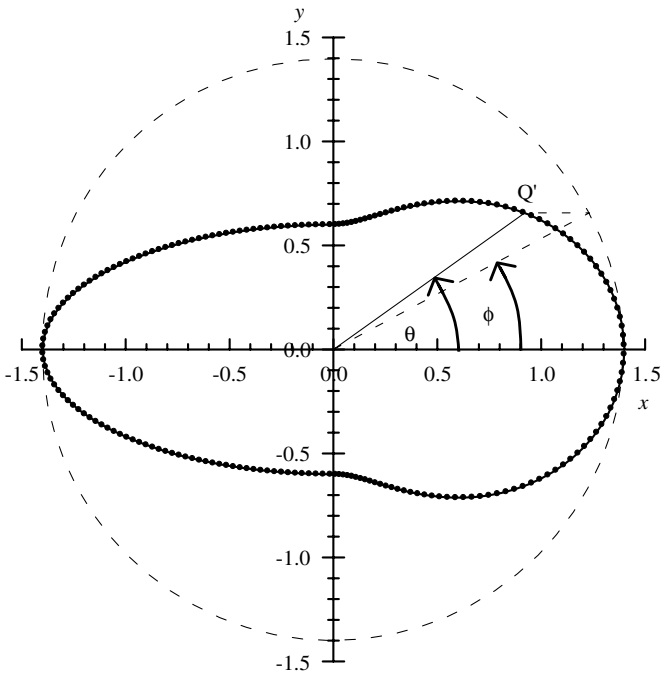

Fig. 11. Irregular crack geometry "Guitel".

ture exactly. Extreme values for the curvature are $\chi_n|_{max} = 2.4169$ for $\theta = 0°$ ($\phi = 0°$), and $\chi_n|_{min} = -0.8895$ for $\theta = 45°$ ($\phi = 35.3483°$).

The crack geometry for the second example is illustrated in Fig. 11. This crack geometry will be referred as "guitel" and it results after the combination of the function

$$r(\theta) = 1 + q \cdot \cos(2 \cdot \theta) \tag{27}$$

with $q = 0.4$ for $-\pi/2 < \theta \leqslant \pi/2$ and an ellipse with aspect ratio $r = 0.4286$ for $\pi/2 < \theta \leqslant 3\pi/2$. This geometry allows studying crack geometries with different aspect ratios and positive and negative curvatures. The crack aspect ratio is $r = 0.5092$ and the maximum and minimum curvatures are $\chi_n|_{max} = 2.6295$ ($\theta = \phi = 0°$) and $\chi_n|_{min} = -1.844$ ($\theta = 90°$ and $\phi = 25.3769°$).

K-results obtained using Calsyf and the original O-integral algorithm were compared to results from BEM computations for the two examples. *K*-computations using BEM were performed following the procedure presented by Cisilino and Aliabadi [25]. For both examples two BEM models with different discretizations were carried out in order to verify the independence of the *K*-results with the model discretization. They are referred

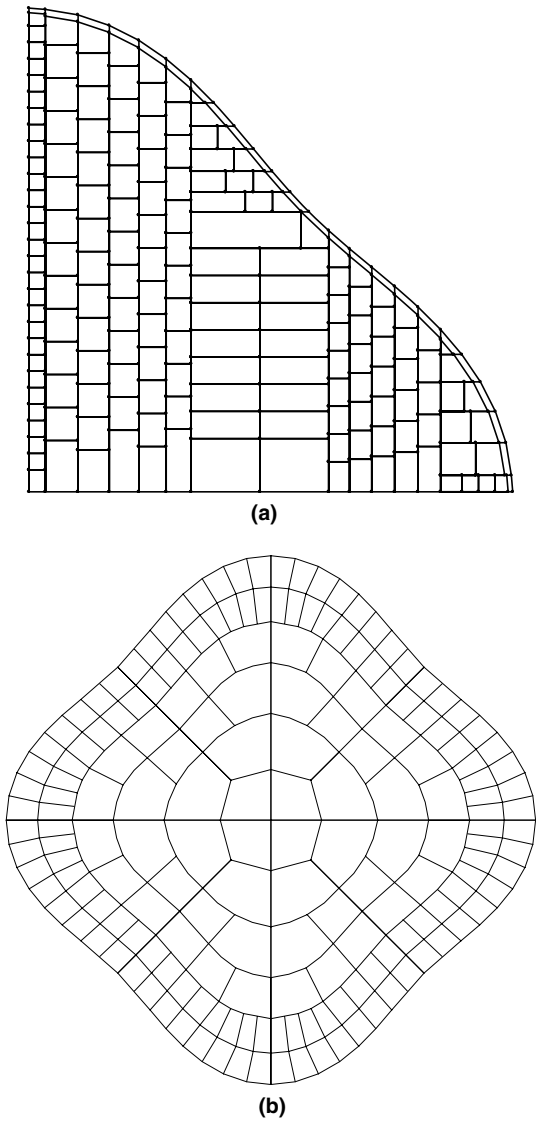

Fig. 12. Model discretizations of Curvan: (a) Calsyf (upper right quarter), (b) BEM model (fine mesh).

in what follows as "coarse" and "fine" meshes. Error of the BEM solution is estimated in a few percent. Model discretizations are depicted in Fig. 12.

Results for the Curvan crack (see Fig. 10) are reported in Fig. 13. Results in Fig. 13(a) corresponds to the loading case $\sigma = \sigma_0$ (uniform stress), while Fig. 13(b) illustrates the results for the loading case $\sigma = \sigma_0 y$ (pure

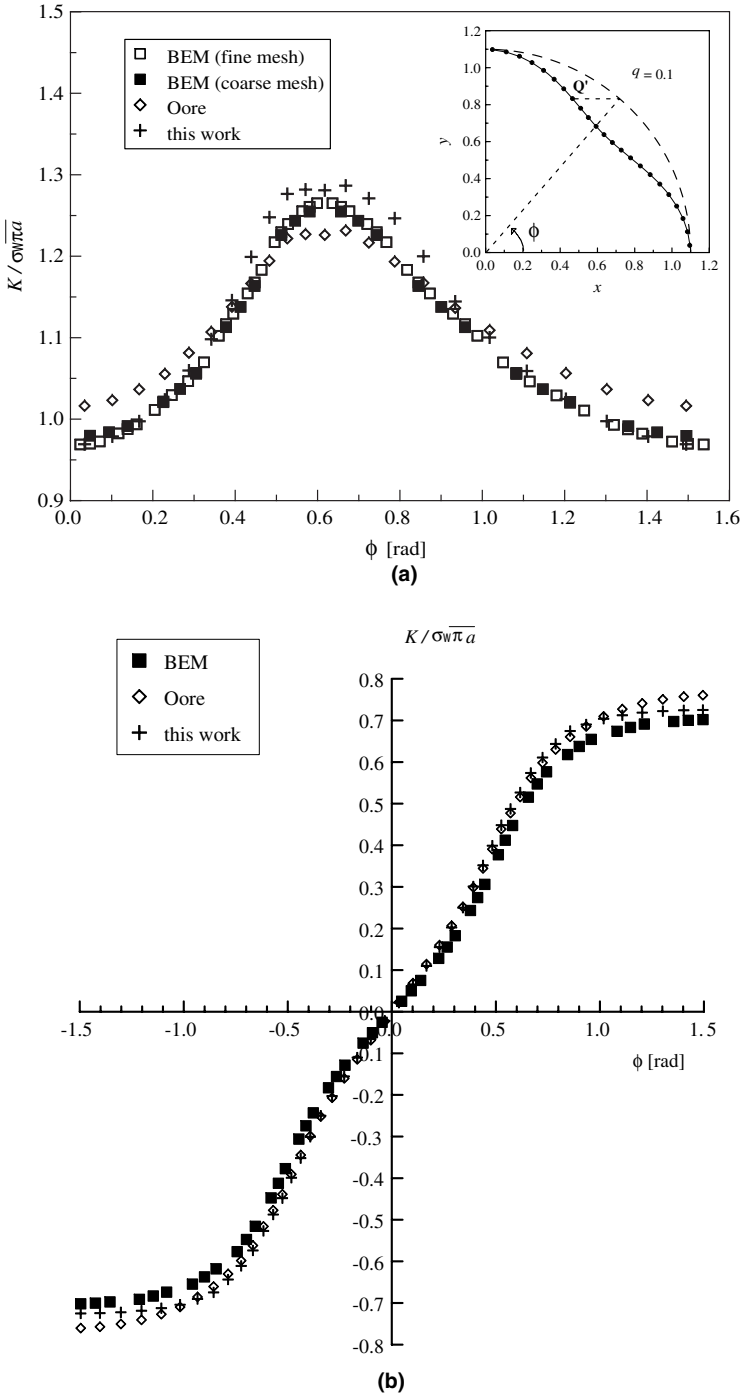

Fig. 13. Normalized K results for the Curvan crack geometry with $q = 0.1$: (a) tension, (b) bending.

Table 1
Normalized Oore, K_{corr} and BEM results at the point of minimum curvature of the Curvan crack geometry under tension

q	Minimum curvature	Normalized K (BEM)	Normalized K (Oore)	Error (%)	This work	Error (%)
0.1	−0.8895	1.2651	1.2261	−3.08	1.2810	1.26
0.2	−4.2754	1.3981	1.3334	−4.63	1.3931	−0.36
0.3	−10.8776	1.5706	1.4058	−10.49	1.4688	−6.48

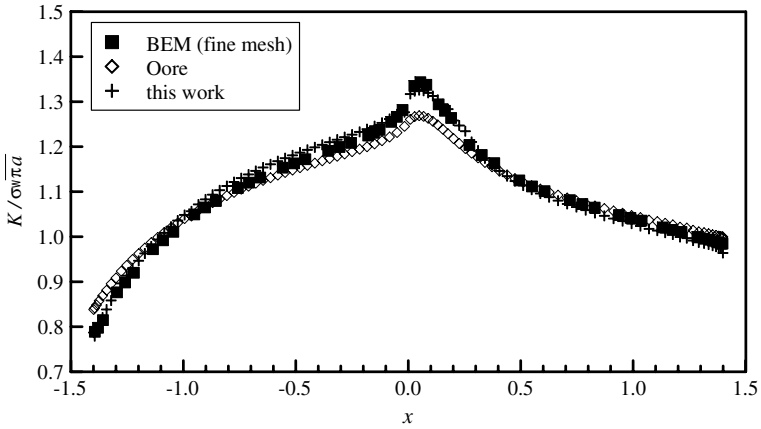

Fig. 14. Normalized K results for Guitel crack geometry with $q = 0.4$ and uniform stress.

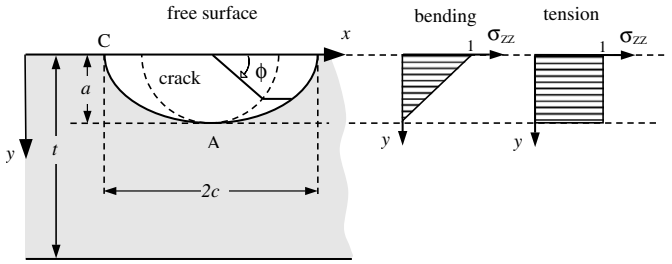

Fig. 15. Semi-elliptical crack under bending and tension. The semi-infinite volume case corresponds to $a/t \to 0$.

Table 2
Normalized K results for the semi-elliptical cracks

Loading case		Tension			Pure bending		
a/c	Point	Isida [26]	Calsyf	e (%)	Isida [26]	Calsyf	e (%)
1.0	A	0.659	0.662	0.46	0.173	0.186	7.5
	C	0.745	0.728	−2.28	–	0.602	–
0.6	A	0.832	0.845	1.56	0.274[a]	0.270	−1.5
	C	–	0.714	–	–	0.595	–

[a] Value for thick plate with $a/t = 0.01$.

bending). Also included in Fig. 13 are the results obtained using the O-integral and those of the BEM computations.

Results for cracks with $q = 0.2$ and $q = 0.3$ are summarized in Table 1. In all cases the errors are calculated with respect to the BEM results obtained using fine mesh in the point with maximum error.

Similarly, results for Guitel corresponding to the loading case $\sigma = \sigma_0$ (uniform stress), are given in Fig. 14.

These results allow to conclude that the proposed corrective function improves the K results obtained using O-integral algorithm when dealing with irregular embedded cracks.

4.2. Surface cracks

The performance of the proposed algorithm is demonstrated in this section for surface cracks in thick and thin plates under tension and bending. The studied geometries are limited to the case of semi-elliptical cracks, as to the author's knowledge, these are the only results available in the literature. The first example consists in a semi-elliptical crack in a semi-infinite volume (see Fig. 15). Two crack aspect ratios are considered, $a/c = 1$

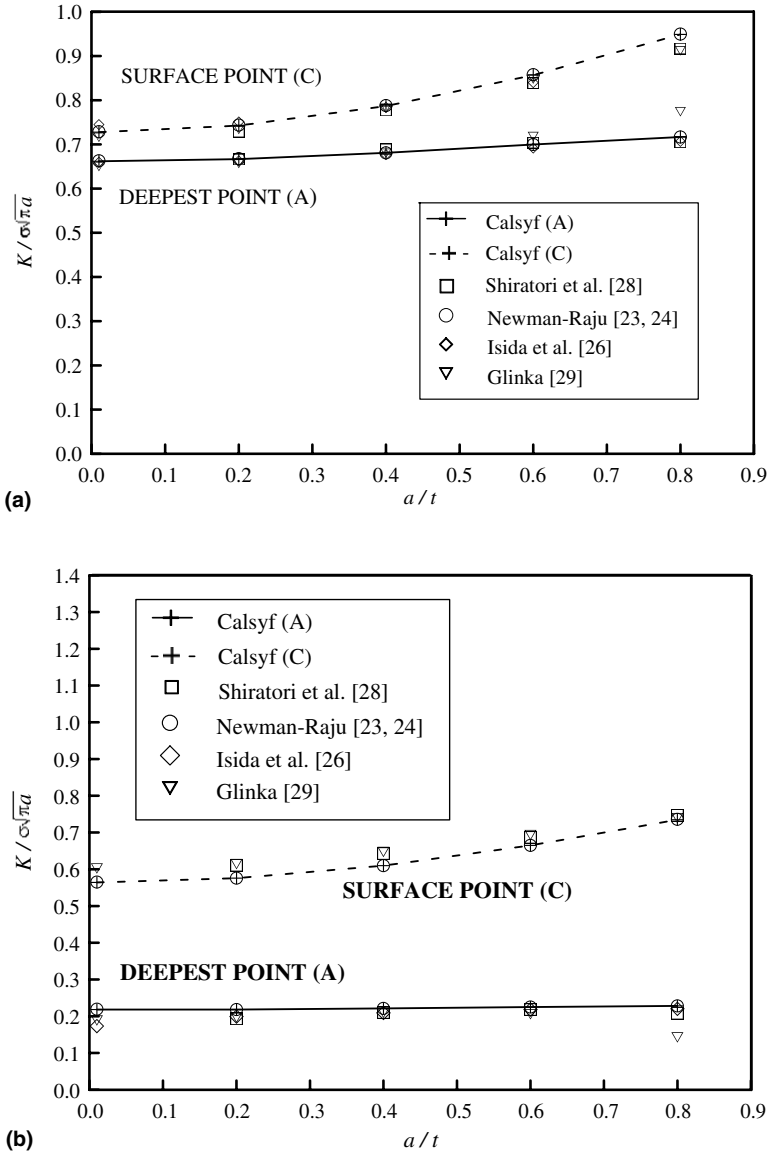

Fig. 16. Normalized K results for the semi-circumference (aspect ratio $a/c = 1$) in a finite plate: (a) tension, (b) bending.

(semi-circular crack) and $a/c = 0.6$. Both geometries are solved subjected to tension and pure bending stress fields. Computed results are reported in Table 2 together with those due to Isida [26] tabulated by Murakami [27]. Results are reported and compared for two positions: points A ($\phi = 90°$) and C ($\phi = 0°$). In all cases results are normalized with respect to $\sigma_0\sqrt{\frac{\pi}{a}}$.

Results computed using Calsyf show an excellent agreement with those of the reference with differences around 2%. The only exception is point A for the semi-circular crack in bending. For this case the difference is 7.5%.

In the second example the effect of finite-thickness is considered. The same crack geometries and loading cases of the first example are studied for plate thickness $a/t = 0.01$, 0.2, 0.4, 0.6 and 0.8. Results for the semi-circular crack are reported in Fig. 16, while the results for the semi-elliptical crack are given in Fig. 17. Results due to Shiratori [28], Isida [26], Glinka [29] and Newman and Raju [23,24] are used for comparison. In all cases the reference results report an accuracy of a few percent.

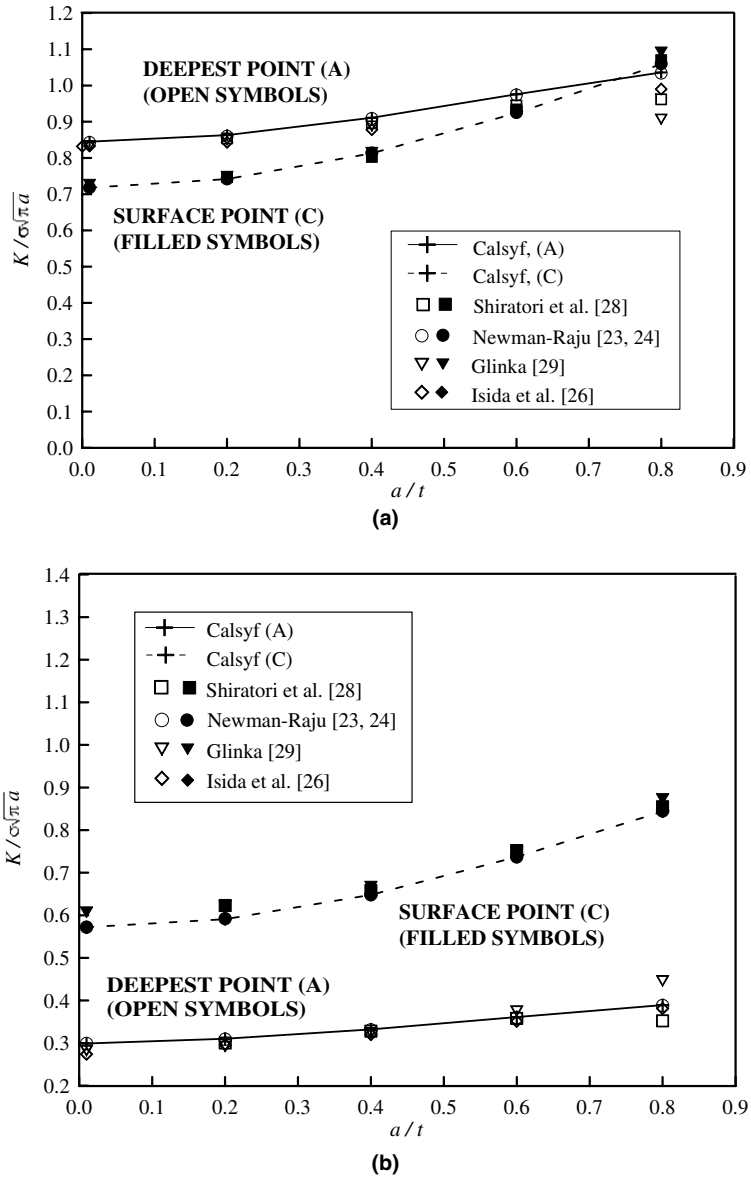

Fig. 17. Normalized K results for the semi-ellipse of aspect ratio 0.6 in finite plate: (a) tension, (b) bending.

Results reported in Figs. 16 and 17 show a very good agreement between the obtained results and those reported in the literature. In particular obtained results are almost coincident to those from Newman and raju [23,24], from which the correction functions for the free surface and finite thickness effects were taken.

5. Conclusions

A numerical tool for the assessment of mode I embedded and surface cracks has been presented in this paper. The proposed tool is an extension of the O-integral algorithm due to Oore and Burns for embedded cracks, which has been effectively extended to deal with cracks of arbitrary shape and surface cracks.

Irregular crack fronts are solved by introducing a corrective function which depends on the crack aspect ratio and the local crack front curvature. Solutions due to Newman and Raju are used to account for the effect of free surfaces and finite thickness. The accuracy of the proposed tool is assessed by solving a number of examples and the results compared to BEM computations and results available in the literature. Obtained results compare well to the reference solutions.

The devised tool constitutes a low-cost and versatile means for computing stress intensity factors for cracks of arbitrary shape. It delivers results within a few percent error while when compared to FEM and BEM models it demands a relatively low computing cost and data preparation.

This work will be extended and customized for the analysis of partially closed cracks and fatigue crack propagation.

Acknowledgements

This work was funded by grants from the Agencia Nacional de Promoción Científica y Técnica de la República Argentina (PICT 12-12528) and the University of Mar del Plata (ING125/03).

Appendix A. Embedded elliptical crack

An empirical K equation for an embedded elliptical crack in a finite plate subjected to remote tension σ, shown in Fig. 18 (see parameter ϕ in Fig. 2), was obtained by Newman and Raju [23]. The equation is

$$K_{\mathrm{I}} = \sigma\sqrt{\frac{\pi \cdot a}{Q}} \cdot F\left(\frac{a}{c}, \frac{a}{t}, \frac{c}{b}, \phi\right) \tag{A1}$$

where

$$Q = 1 + 1.464\left(\frac{c}{a}\right)^{1.65} \tag{A2}$$

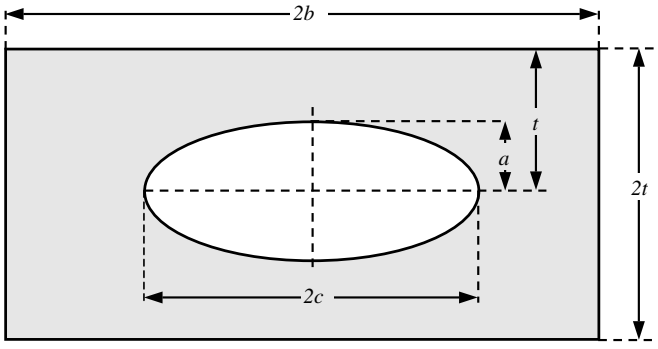

Fig. 18. Embedded elliptical crack configuration.

and

$$F = \left[M_1 + M_2\left(\frac{a}{t}\right)^2 + M_3\left(\frac{a}{t}\right)^4\right] \cdot g \cdot f_w \cdot f_\phi \tag{A3}$$

The function f_ϕ was taken from the exact solution for an embedded elliptical crack in an infinite solid [18], f_w is a finite-width correction factor, and the function g is a fine-tuning curve-fitting function. For $a/c \leqslant 1$, the functions are expressed by

$$M_1 = 1 \tag{A4}$$

$$M_2 = \frac{0.05}{0.11 + \left(\frac{a}{c}\right)^{3/2}} \tag{A5}$$

$$M_3 = \frac{0.29}{0.23 + \left(\frac{a}{c}\right)^{3/2}} \tag{A6}$$

$$g = 1 - \frac{\left(\frac{a}{t}\right)^4}{1 + 4\left(\frac{a}{c}\right)} \cdot |\cos\phi| \tag{A7}$$

$$f_w = \left[\sec\left(\frac{\pi c}{2b}\right)\sqrt{\frac{a}{t}}\right]^{1/2} \tag{A8}$$

$$f_\phi = \left[\left(\frac{a}{c}\right)^2 \cos^2\phi + \sin^2\phi\right]^{1/4} \tag{A9}$$

From the above equations, the limiting case of the elliptical crack embedded in an infinite volume under remote tension (i.e., when $a/t \to 0$) is expressed by

$$Y_b = \frac{K_I}{\sigma\sqrt{\pi a}} = \frac{f_\phi}{\sqrt{Q}} \tag{A10}$$

Appendix B. Semi-elliptical surface crack in a finite width plate

The case of a semi-elliptical surface crack in a finite plate subjected to tension and bending was solved in another work of Newman and Raju [24] (see Fig. 19(a) and (b) for details). The K equation for combined tension and bending loads is

$$K_I = (\sigma_m + H \cdot \sigma_b)\sqrt{\frac{\pi \cdot a}{Q}} \cdot F_S\left(\frac{a}{c}, \frac{a}{t}, \frac{c}{b}, \phi\right) \tag{B1}$$

where σ_m represents the remote uniform-tension stress, and σ_b the remote outer-fiber bending stress. The Q factor was given in Appendix A, and the function F_S has a similar expression:

$$F_S = \left[M_1^S + M_2^S\left(\frac{a}{t}\right)^2 + M_3^S\left(\frac{a}{t}\right)^4\right] \cdot g_S \cdot f_w \cdot f_\phi \tag{B2}$$

The functions f_w and f_ϕ are the functions already given in Appendix A. The other functions in the above equation are expressed by

$$M_1^S = 1.13 - 0.09\left(\frac{a}{c}\right) \tag{B3}$$

$$M_2^S = -0.54 + \frac{0.89}{0.2 + \left(\frac{a}{c}\right)} \tag{B4}$$

$$M_3^S = 0.5 - \frac{1.0}{0.65 + \left(\frac{a}{c}\right)} + 14\left(1.0 - \frac{a}{c}\right)^{24} \tag{B5}$$

$$g_S = 1 + \left[0.1 + 0.35\left(\frac{a}{t}\right)^2\right] \cdot (1 - \sin\phi)^2 \tag{B6}$$

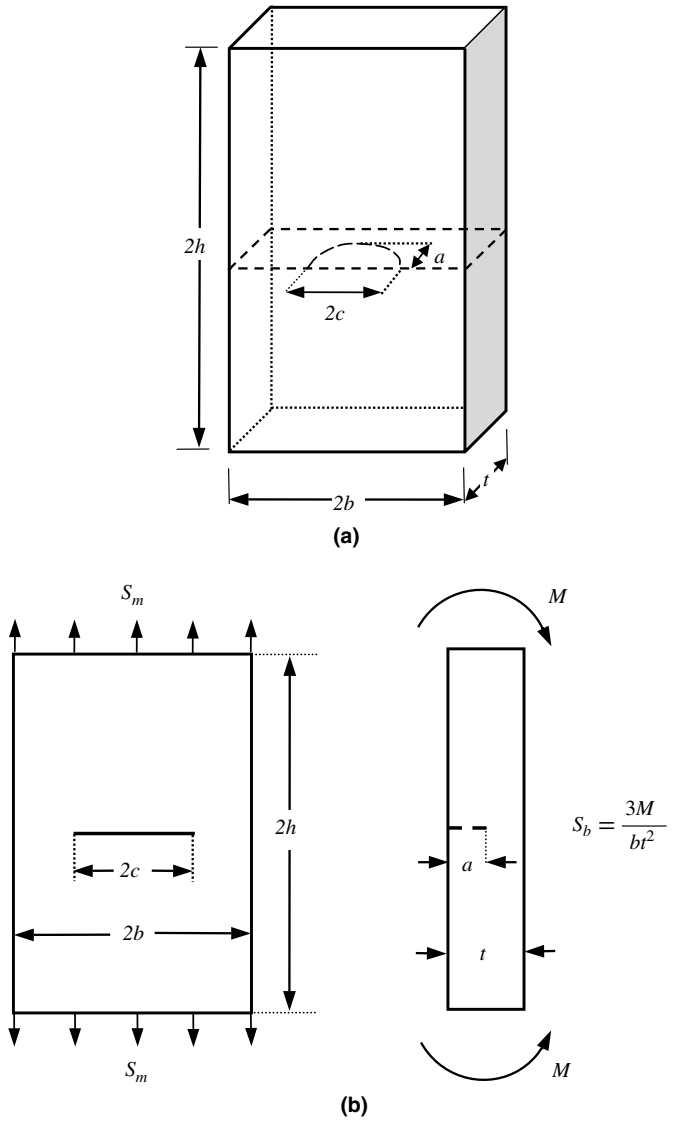

Fig. 19. (a) Elliptical surface crack in a finite plate, (b) surface-cracked plate subjected to tension or bending loads.

The function H has the form

$$H = H_1 + (H_2 - H_1)\sin^p \phi \tag{B7}$$

where

$$p = 0.2 + \frac{a}{c} + 0.6\frac{a}{t} \tag{B8}$$

$$H_1 = 1 - 0.34\frac{a}{t} - 0.11\frac{a}{c}\left(\frac{a}{t}\right) \tag{B9}$$

$$H_2 = 1 + G_1\left(\frac{a}{t}\right) + G_2\left(\frac{a}{t}\right)^2 \tag{B10}$$

In this equation for H_2

$$G_1 = -1.22 - 0.12\left(\frac{a}{c}\right) \tag{B11}$$

$$G_2 = 0.55 - 1.05\left(\frac{a}{c}\right)^{0.75} + 0.47\left(\frac{a}{c}\right)^{1.5} \tag{B12}$$

The limit case of a semi-elliptical surface crack in a semi-infinite volume under uniform remote tension gives (i.e., $\sigma_b = 0$), from the above equations:

$$K_I = \sigma_m\sqrt{\frac{\pi \cdot a}{Q}} \cdot [1.13 - 0.09(a/c)]\left(1 + 0.1(1 - \sin\phi)^2\right) \cdot f_\phi \tag{B13}$$

taking account of Eq. (A10) in Appendix A, the above equation can be expressed by

$$Y = \frac{K_I}{\sigma_m\sqrt{\pi a}} = \lambda_s \cdot Y_b \tag{B14}$$

with

$$\lambda_s = [1.13 - 0.09(a/c)]\left(1 + 0.1(1 - \sin\phi)^2\right) \tag{B15}$$

References

[1] American Society of Mechanical Engineers (ASME) Boiler and Pressure Vessel Code. Section IX: Rules for Inservice Inspection of Nuclear Power Plant Components. New York: American Society of Mechanical Engineers, September 2004.
[2] PD 6493: 1991. Guidance on some methods for the derivation of acceptance levels for defects in fusion welded joints, British Standards Institution, August 1991.
[3] Harrison RP, Loosemore K, Milne I, Dowling AR. Assessment of the integrity of structures containing defects. CEGB R6, Rev 2 1980.
[4] Kumar V, German MD, Shih CF. An engineering approach for elastic-plastic fracture analysis. EPRI Report NP-1931, Palo Alto, CA: Electric Power Research Institute, 1981.
[5] EPRI Report GS-6724. Condition assessment guidelines for fossil fuel power plant components. USA: Electric Power Research Institute, 1990.
[6] BS 7910. Guidance on methods for assessing the acceptability of flaws in metallic structures. London, UK: British Standard Institution, 1999.
[7] Pisarski H, Wallin K. The SINTAP fracture toughness estimation procedure. The Welding Institute; 2000.
[8] API recommended Practice 579, Fitness for Service, 1st ed., American Petroleum Institute, August 2000.
[9] Murakami Y, Namat-Nasser S. Growth and stability of surface flaws of arbitrary shape. Engng Fract Mech 1983;17(3):193–210.
[10] Murakami Y. Analysis of stress intensity factors of modes I, II and III for inclined surface cracks of arbitrary shape. Engng Fract Mech 1985;22(1):101–14.
[11] Noda N-A. Stress intensity formulas for three-dimensional cracks in homogeneous and bonded dissimilar materials. Engng Fract Mech 2004;71:1–15.
[12] Aliabadi MH, Rooke DP. Numerical fracture mechanics. Kluwer Academic Publishers; 1991.
[13] Bueckner HF. A novel principle for the computation of stress intensity factors. Z Angew Math Mech 1970;50:529.
[14] Rice JR. Some remarks on elastic crack-tip stress fields. Int J Solid Struct 1972;8:751.
[15] Wu Xue-Ren, Carlsson AJ. Weight functions and stress intensity factor solutions. 1st ed. Pergamon Press; 1991.
[16] Oore M, Burns DJ. Estimation of stress intensity factors for embedded irregular cracks subjected to arbitrary normal stress fields. Trans ASME 1980;102(May):202–11.
[17] Desjardins JL, Burnsy DJ, Thompson JC. A weight function technique for estimating stress intensity factors for cracks in high pressure vessels. J Pressure Vessel Technol 1991;113(1):55–64.
[18] Irwin GR. The crack extension force for a part-through crack in a plate. ASME J Appl Mech 1962:651–4.
[19] Shah RC, Kobayashi AS. Stress intensity factor for an elliptical crack under arbitrary normal loading. Engng Fract Mech 1971;3:71–96.
[20] Isida M, Yoshida T, Noguchi H. Prelim. In: Proc Japan Soc Mech Engrs and Japan Soc Precision Engng, Mie District, No. 823-3, 1982. p. 15–7.
[21] Oore M, Burns DJ. Estimation of stress intensity factors for irregular cracks subjected to arbitrary normal stress fields. In: Proceeding of the 4th international conference on pressure vessel technology, London, I Mech. E, vol. 1, 1980. p. 139–47.
[22] Grueter L, Huget W, Kylla H. Weight functions and stress intensity magnification factors for elliptical and semi-elliptical cracks under variable normal stress. Interatom Report INTAT No. 32.05095.0, May 1981.

[23] Newman JC, Raju IS. An empirical stress intensity factor equation for the surface crack. Engng Fract Mech 1981;15(1):185–92.
[24] Newman JC, Raju IS. Stress intensity factor equations for cracks in three-dimensional finite bodies. Fracture mechanics: 14th symposium – theory and analysis. In: Lewis JC, Sines G, editors. ASTM STP 791, vol. I. American Society for Testing and Materials; 1983. p. I-238–65.
[25] Cisilino AP, Aliabadi MH. Three-dimensional BEM analysis for fatigue crack growth in welded components. Int J Pressure Vessels Piping 1997;70:135–44.
[26] Isida M, Noguchi H, Yoshida Y. Tension and bending of finite thickness plates with a semi-elliptical surface crack. Int J Fract 1984;26:157–88.
[27] Murakami Y. Stress intensity factors handbook. The Society of Materials Science. Japan: Pergamon Press; 1990.
[28] Shiratori M, Miyoshi T, Tanikawa K. Analysis of stress intensity factors for surface crack subjected to arbitrarily distributed surface stresses (2nd report, Analysis and application of influence coefficients for flat plates with a semi-elliptical surface crack). Trans Jpn Soc Mech Engrs 1986;52(474):390–8.
[29] Glinka G. AFGROW program, ver. 4.0004.12.10. AFGROW web site, public service by the Analytical Structural Mechanics Brand, Air Vehicles Directorate, US Air Force Research Laboratory.